

## MYSTIC: a high angular resolution K-band imager at CHARA

Benjamin R. Setterholm<sup>1, a, b, \*</sup>, John D. Monnier<sup>1, a</sup>, Jean-Baptiste Le Bouquin<sup>1, c</sup>,  
Narsireddy Anugu<sup>1, d</sup>, Jacob Ennis<sup>1, a</sup>, Laurent Jocou<sup>1, c</sup>, Nour Ibrahim<sup>1, a</sup>,  
Stefan Kraus<sup>1, e</sup>, Matthew D. Anderson<sup>1, d</sup>, Sorabh Chhabra<sup>1, e</sup>, Isabelle Codron<sup>1, e</sup>,  
Christopher D. Farrington<sup>1, d</sup>, Becky Flores<sup>1, f</sup>, Tyler Gardner<sup>1, a, e</sup>, Mayra Gutierrez<sup>1, a</sup>,  
Cyprien Lanthermann<sup>1, d</sup>, Olli W. Majoinen<sup>1, d</sup>, Daniel J. Mortimer<sup>1, e</sup>, Gail Schaefer<sup>1, d</sup>,  
Nicholas J. Scott<sup>1, d</sup>, Theo ten Brummelaar<sup>1, d</sup> and Norman L. Vargas<sup>1, d</sup>

<sup>a</sup>University of Michigan, Department of Astronomy, Ann Arbor, Michigan, United States

<sup>b</sup>University of Michigan, Department of Climate and Space Sciences and Engineering, Ann Arbor, Michigan, United States

<sup>c</sup>Institut de Planétologie et d'Astrophysique de Grenoble, Grenoble, France

<sup>d</sup>CHARA Array of Georgia State University, Mount Wilson Observatory, Mount Wilson, California, United States

<sup>e</sup>University of Exeter, Department of Physics and Astronomy, Exeter, United Kingdom

<sup>f</sup>Georgia State University, Department of Physics and Astronomy, Atlanta, Georgia, United States

**ABSTRACT.** The Michigan Young Star Imager at CHARA (MYSTIC) is a K-band interferometric beam combining instrument funded by the U.S. National Science Foundation, designed primarily for imaging sub-au scale disk structures around nearby young stars and to probe the planet formation process. Installed at the CHARA Array in July 2021, with baselines up to 331 m, MYSTIC provides a maximum angular resolution of  $\lambda/2B \sim 0.7$  mas. The instrument injects phase-corrected light from the array into inexpensive, single-mode, polarization maintaining silica fibers, which are then passed via a vacuum feedthrough into a cryogenic dewar operating at 220 K for imaging. MYSTIC uses a high frame rate, ultra-low read noise SAPHIRA detector and implements two beam combiners: a six-telescope image plane beam combiner, based on the MIRC-X design, for targets as faint as 7.7 Kmag, as well as a four-telescope integrated optic beam-combiner mode using a spare chip leftover from the GRAVITY instrument. MYSTIC is co-phased with the MIRC-X (J + H band) instrument for simultaneous fringe-tracking and imaging and shares its software suite with the latter to allow a single observer to operate both instruments. We present the instrument design, review its operational performance, present early commissioning science observations, and propose upgrades to the instrument that could improve its K-band sensitivity to 10th magnitude in the near future.

© The Authors. Published by SPIE under a Creative Commons Attribution 4.0 International License. Distribution or reproduction of this work in whole or in part requires full attribution of the original publication, including its DOI. [DOI: [10.1117/1.JATIS.9.2.025006](https://doi.org/10.1117/1.JATIS.9.2.025006)]

**Keywords:** optical interferometry; K band; protoplanetary disks

Paper 22103G received Oct. 24, 2022; revised Apr. 7, 2023; accepted May 18, 2023; published Jun. 6, 2023.

### 1 Introduction

Interferometric arrays enable the study of astrophysical phenomena at significantly higher angular resolution than monolithic observatories alone. By simultaneously collecting light at multiple stations and coherently combining the signals together, the spatial extent of distant sources can be inferred from the resulting interference patterns by mapping measured fringe visibilities and

\*Address all correspondence to Benjamin Setterholm, [bensett@umich.edu](mailto:bensett@umich.edu)

baseline separations to the Fourier plane and inverting to image space. This technique has proved to be remarkably successful in recent decades at radio wavelengths, where measurements of the electromagnetic field can be mixed and amplified with electrical signals and then correlated *in situ* using contemporary electronics or digitized for *ex post facto* correlation in software. For such arrays, the incorporation of additional receivers is largely a matter of material and computational cost. At shorter wavelengths however, long baseline interferometry is currently only feasible by guiding and directly interfering light through an optical system in real time. Owing to the losses inherent in such optical systems with many reflections, near-infrared and visible light long-baseline interferometers are limited to combining light from only a small number of telescopes simultaneously in order to attain statistically significant visibility signal-to-noise ratios.

The largest operational optical interferometer is the Center for High Angular Resolution Astronomy (CHARA) Array,<sup>1</sup> located on Mount Wilson, California. This facility consists of six 1-m telescopes in a Y-shaped configuration, spanning baseline separations ranging from 34 to 331 m, and is equipped with adaptive optics (AO) systems at each telescope and within the beam-combination laboratory to improve the flux injection into the facility instruments (see Refs. 2–4). Whereas most beam-combining instruments at CHARA only use a subset of the Array telescopes at a time for improved sensitivity, the Michigan InfraRed Combiner (MIRC)<sup>5</sup> (commissioned in fall 2005) was designed to collect simultaneous fringes from all 15 baseline pairs across the near-infrared (J, H, and K bands). With new scientific opportunities made available by the expanded *uv*-plane coverage, MIRC quickly became the predominant instrument at CHARA.

In June 2017, the MIRC camera, featuring a Rockwell PICNIC detector array, was supplanted by a C-RED One camera from First Light, employing an ultra-high speed, sub-electron read noise, HgCdTe avalanche photodiode SAPHIRA detector.<sup>6</sup> This upgrade, funded by the European Research Council, provided a  $>1$  Hmag sensitivity improvement for faint and extended objects.<sup>7</sup> Concurrently, the image plane beam combiner was redesigned to operate at room temperature, with the replacement combiner using single-mode, polarization maintaining optical fibers and an 80/20 beam splitter for recording photometric information of each beam. These improvements allowed the photometric signal to be robust to temporal drifts and reduced instrumental polarization effects. However, since the beam-combining optics were no longer kept inside a cryogenic dewar, the upgraded instrument was limited to operate at J and H bands only due high thermal background in the K band. Over the next year, most of the remaining optics in the beam train were updated culminating in the rebranded MIRC-X instrument,<sup>8</sup> fully commissioned in September 2018.

The Michigan Young Star Imager at CHARA (MYSTIC) was designed alongside the MIRC-X upgrade and by the same team. MYSTIC is a cryogenic, K-band (1.95 to 2.38  $\mu\text{m}$ ) instrument utilizing a C-RED One camera like its sister instrument MIRC-X. Two different beam combiners reside within the MYSTIC cryostat: a six-telescope all-in-one (AIO) image plane combiner with photometric channels and a four-telescope pairwise (ABCD) photonic integrated circuit combiner. MIRC-X and MYSTIC share an optical bench at CHARA; whereas it is possible to operate the each instrument independently, both instruments use a shared software architecture enabling a single observer to control both instruments simultaneously. MYSTIC was first commissioned on-sky in July 2021, and the AIO mode was made immediately available to all observers with MIRC-X programs. The ABCD mode hardware was later added in May 2022.

## 2 Scientific Drivers

MYSTIC was designed from its conception to operate in tandem with the J/H-band MIRC-X instrument, enabling robust fringe tracking even if one of the instruments is measuring near a visibility null. Leveraging all 15 simultaneous baselines and 20 closure triangles available at CHARA, MIRC-X and MYSTIC together sample a larger portion the *uv*-plane at higher spatial resolution than any other current long-baseline facility in a single pointing. This opens new avenues for high angular resolution astronomical research not possible with other instrument facilities, particularly in the realm of model independent imaging. An example of the *uv*-coverage available in a single night's observing with MIRC-X and MYSTIC is shown in Fig. 1.

MYSTIC's primary *raison d'être* is the study of the inner-au regions of protoplanetary disks surrounding young stellar objects (YSOs). MIRC-X has demonstrated its ability to observe

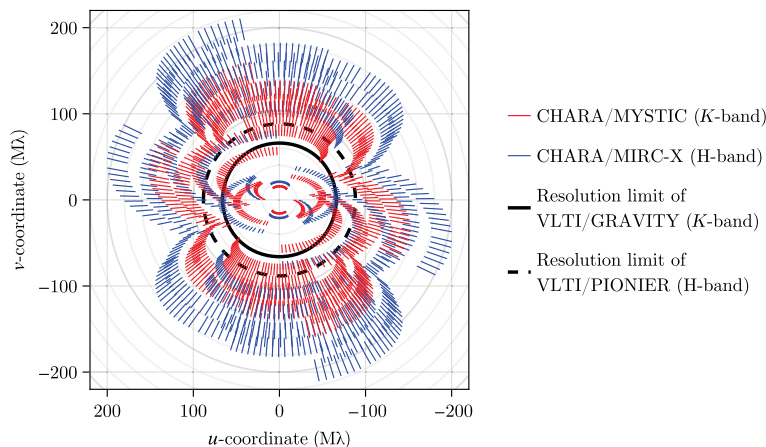


**Fig. 1** A sample  $uv$ -plane track available in a single night for the Herbig Ae/Be star AB Aurigae. (Note that this figure does not include overheads for collecting calibration data; realistically, this  $uv$ -coverage is attainable over the course of two nights.) Utilizing all six CHARA telescopes, MIRC-X and MYSTIC can collect more simultaneous data at higher angular resolutions than any other currently available near-infrared interferometer facility.

interferometric fringes for dozens of Herbig Ae/Be (young intermediate-mass stars,  $2M_{\odot} - 10M_{\odot}$ ) systems at low spectral resolution ( $R \sim 50$  to  $100$ ). Coordinated observations with MYSTIC will expand the Fourier and spectral coverage of all of these targets into the K-band, providing sufficient information for regular snapshot image reconstructions. Furthermore, MYSTIC will enable the study of several T Tauri targets (young solar analogues,  $<2M_{\odot}$ ), which are generally too faint for reliable fringe tracking with MIRC-X alone. The wide spectral band coverage provided by MIRC-X and MYSTIC together will facilitate the identification and characterization of a variety of YSO disk features including: warps and inner-disk misalignments, signatures of orbiting objects, localized vorticities and other disk anomalies, as well as distinguishing between gas- or dust-dominated emission in the stellar accretion zone. YSO studies with these instruments will critically inform planet formation models and reveal temporal phenomena responsible for shadowing variability seen in stellar disks on large scales. Figure 2 shows the population of YSO targets in the nearby Taurus star-forming region and the

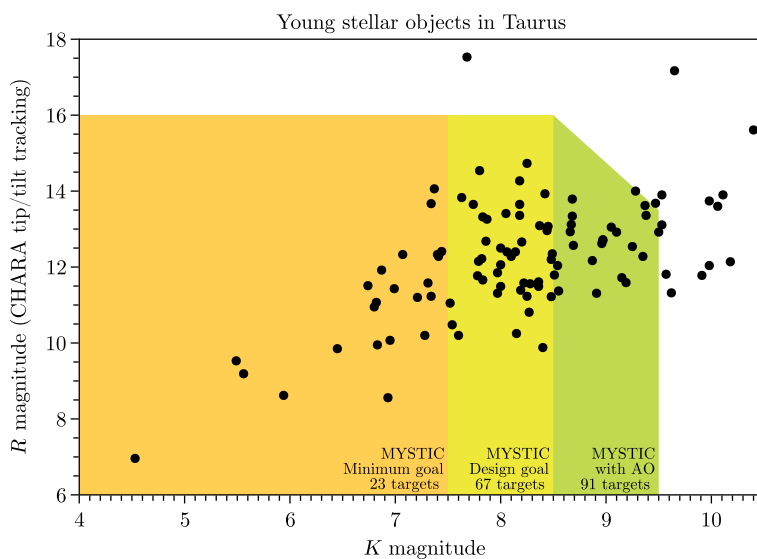


**Fig. 2** Required instrumental sensitivity to observe YSO targets in the Taurus-Auriga molecular cloud region,<sup>9</sup> which drove the design specification of MYSTIC. Currently, MYSTIC as-built meets the minimum specification (orange region). Planned future upgrades (see Sec. 10) will deliver an increase of at least 1 magnitude in sensitivity (yellow region) which more than doubles the number of available objects for study.

number of targets that would be available to MYSTIC at a given sensitivity. Previous observations have shown that many nearby YSO disk systems tend to be very resolved at the longer CHARA baselines. Although these sources tend to be brighter overall in the K-band compared to H-band, the stellar contribution to the overall flux is significantly lower, leading to fringe contrasts often below 10%. To accomplish the aforementioned goals, particularly probing T Tauri objects, we require that MYSTIC be capable of observing YSO targets at 7.5 magnitude or fainter in the K band.

By including a handful of higher spectral resolution dispersion elements, the design requirements driving MYSTIC for YSO imaging make the instrument suitable for a few secondary science objectives as well. CHARA's baselines, coupled with the availability of intermediate spectral resolutions ( $R \sim 200$  to  $1000$ ) in MYSTIC, open up the possibility of high precision closure phase and differential phase measurements for  $\sim 5$ th Kmag and brighter targets after careful nightly wavelength calibration with the ARMADA etalon module.<sup>10</sup> For binary systems, these measurements can be used for microarcsecond-precision astrometry, enabling the direct detection of Jovian exoplanets, where the K-band flux contrast between planet and host star is more favorable compared to the shorter wavelengths available to MIRC-X. The spatial resolution afforded by CHARA's baselines will make it possible to disentangle the spectral contributions of the star and planet components, allowing for broad characterization of giant planet atmospheres in the near infrared.

Within the K-band, spatial resolution of prominent Br- $\gamma$  ( $2.166 \mu\text{m}$ ) and CO overtone emission ( $2.28$  to  $2.35 \mu\text{m}$ ) of Herbig Ae/Be targets will enable study of the star-disk connection by probing magnetically driven accretion flows; MYSTIC is thus also designed to facilitate medium spectral resolution ( $R \sim 2000$ ) observations. Though such a high spectral resolution would not provide a sufficient signal-to-noise ratio to observe targets of astrophysical interest with MYSTIC alone, given the stochastic millisecond-timescale phase delays induced by atmospheric turbulence, concurrent operation of MIRC-X as a high-precision optical delay tracker at a lower spectral resolution could greatly extend MYSTIC's exposure times (to the order of seconds or even minutes). Conversely, high-precision fringe tracking with MYSTIC will enable velocity integrated imaging of more prominent spectral lines in the J and H bands accessible by MIRC-X.

### 3 Technical Requirements

Driven by the science goals mentioned in the previous section, as well as necessary interfacing with MIRC-X and CHARA at large, the following technical requirements constraining the design for the MYSTIC instrument were defined.

1. The detector must deliver a fast readout ( $>300$  Hz) with low noise to allow for coherent integration of fringe visibilities with a high signal-to-noise ratio.
2. The instrument must provide a cryogenic subsystem operating at 220 K for the combiner optics to minimize thermal background in the K band.
3. The cold and warm optic systems shall be connected by single-mode, polarization-maintaining fiber optics to provide spatial filtering. These fibers must provide  $>50\%$  overall throughput at all wavelengths in the science bandpass.
4. The instrument design must support a six-beam AIO combiner as well as a spare four-beam integrated optic combiner chip<sup>11</sup> from the GRAVITY instrument.
5. The entire beam-train and supporting hardware must reside on (or above) the shared optical bench with the MIRC-X instrument while minimizing the total number of reflections.
6. MYSTIC must provide six-beam pairwise interference with sensitivity to track fringes with minimal cross-talk at modest spectral resolution ( $R \sim 50$ ) of YSO disks as faint as at least Kmag = 7.5, with a goal of fringe tracking objects as faint as 8.5 Kmag.
7. The operating software for MYSTIC must integrate tightly with the MIRC-X instrument for coordinated fringe tracking and data collection. A single observer should be able to control both instruments simultaneously with minimal additional burden compared to operating a single instrument alone.

8. To optimize for the image reconstruction of at least 20 T Tauri objects and to facilitate the interpretation of temporally varying sources, we require a calibration precision of  $<2\%$  for square visibility and  $<0.1$  deg for closure phase measurements at a spectral resolution of at least  $R = 20$ .
9. At least one strong emission line should be resolvable, ideally probing hot gas near the wind-launching region of YSO sources.
10. MYSTIC must be fully automated system to enable remote operations, including failsafe mechanisms in case of power outages to protect the detector and cryogenic optics. We also require a daily, automatic assessment, and report of system health.

## 4 Instrument Overview

A high-level schematic of the MYSTIC instrument layout is presented in Fig. 3. The entire footprint of the MYSTIC instrument fits on a shared optical bench with MIRC-X in the CHARA beam lab. For reference, we note here that the collimated light beams provided by the array are separated 3 in. apart, have a diameter of 19 mm, and include an optical path delay (OPD) of 11.2 in. between successive beams. The common MIRC-X/MYSTIC optical bench is located 6 in. below the center of each of the beams. MYSTIC's optical train is divided into two subsystems: a warm optics system, operating at room temperature, and a cold optics system, operating in a cryogenic vacuum dewar. The warm optics system (see Sec. 5) steers the infrared light beams issuing from the CHARA Array, correcting for beam drift, differential birefringence, and group delay, into a series of commercially available, single-mode, polarization-maintaining silica fiber optics. These fibers transport the light into the cold optics system (see Sec. 7), which conducts interferometric beam combination, spectral dispersion, and photon detection. The cold optics cryostat is positioned so that it does not interfere with JouFLU<sup>12</sup> instrument operations.

MYSTIC provides several combinations of possible observing modes—namely, the choice of beam combiner and dispersion optic(s)—many of which are made available to the general community without any additional support necessary. A few modes still remain under development by the instrument team and their use for active science will be considered on a case-by-case basis until they are made fully available to the public. In particular, MYSTIC's cryostat contains two distinct beam combiners: an AIO six-telescope image plane combiner, based on the design of MIRC-X (see Sec. 7.1), and a cross-talk resistant, four-telescope, pairwise integrated optic chip

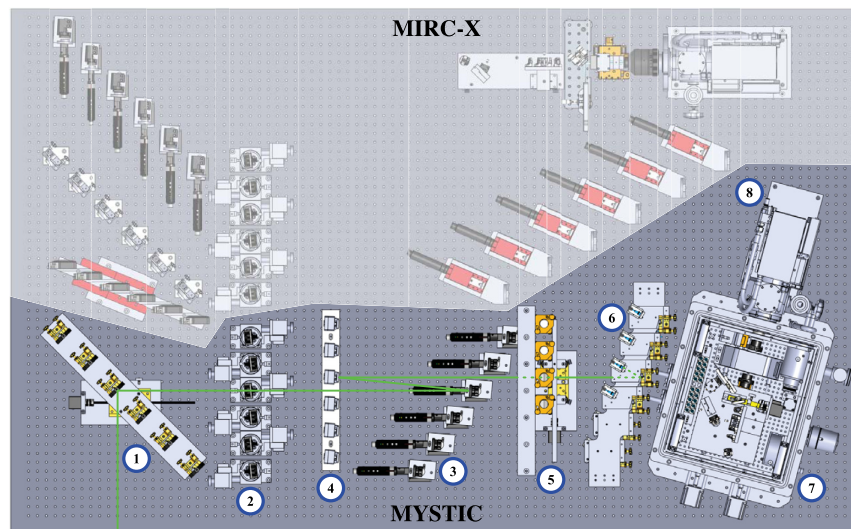


**Fig. 3** Schematic diagram of the MIRC-X/MYSTIC optical bench. The MIRC-X instrument on the southern side of the table (top) is faded out to draw attention to MYSTIC. A green line indicates the optical path through the warm optic train along one of the beams. Labeled elements in MYSTIC are as follows: (1) dichroic pickoff assembly, (2) polarization control modules, (3) differential delay lines, (4) tip/tilt control modules, (5) periscope, (6) fiber injection modules, (7) cryostat and cold optic system, and the (8) C-RED one camera.

combiner (ABCD), which was initially created as a spare for the VLTI/GRAVITY instrument<sup>13</sup> (see Sec. 7.2). These combiners are fed by exclusive sets of fiber optics, with light injection dictated by the state of the periscope assembly in the warm optics system. Currently, the ABCD mode combiner is not fully supported in the operational software of MIRC-X/MYSTIC and not at all supported as of yet in the data reduction software. With regards to the dispersion optics, all spectral-dispersing optics are available, but use of the Wollaston prism on-sky for polarimetric observations is discouraged owing to the lack of wave-plate optics in the beam-train necessary to conduct true spectro-polarimetric measurements. Furthermore, the divergence angle of the Wollaston prism ( $\sim 1$  deg) excludes its utility in conjunction with any of the grism optics. (The Wollaston prism is included primarily for fine-tuning the polarization control module orientations in the warm optics system during routine instrument alignment. A full polarimetric observing mode may someday be added to MYSTIC if interest and funding become available, as was the case for MIRC-X.<sup>14</sup>)

MYSTIC has repeatedly demonstrated a fringe tracking limiting magnitude on-sky of 7.5 with the  $R = 50$  prism under good seeing conditions (with a record of 7.7 during a night with especially excellent atmospheric seeing operating in tandem with MIRC-X). We note that visibility measurements of objects fainter than this magnitude are still feasible, provided that the target is bright enough in the H band for fringe tracking with MIRC-X. Table 1 enumerates the expected limiting AIO mode K-band correlated magnitudes for MYSTIC fringe tracking at all supported spectral modes, based partially on observed performance on-sky during commissioning as well as relative performance with the internal CHARA Six Telescope Simulator (STS)<sup>8</sup> calibration light source. At the time of writing, detailed estimates of the ABCD mode limiting magnitudes are not yet available; preliminary on-sky tests demonstrate that this mode can obtain visibility measurements for targets at least as faint as the magnitude limiting cases for the AIO mode.

MYSTIC is fully motorized so that observers can operate the instrument entirely remotely. MIRC-X and MYSTIC use a shared software architecture and MYSTIC adopts nearly the same GUIs as those already familiar to users of MIRC-X; even subsystems with different hardware implementations between the two instruments, such as the fiber injection strategy, provide a uniform interface for the observer. Both instruments use a single, common GUI for data collection and high-level observing tasks. A continually running server logs the vacuum status, temperature, vibration, hard drive usage, and camera status of both instruments, and an automatic system health summary is generated every 12 hours and posted to an internal Slack channel.

The real-time software allows either MIRC-X or MYSTIC to act as the “primary” instrument, controlling the CHARA delay line carts and maintaining phase delay tracking for itself, with the “secondary” instrument managing its own group delay via dedicated linear actuators

**Table 1** Estimated AIO mode limiting magnitudes without MIRC-X fringe tracking.

Optic(s)	$R$	Kmag
Prism	20	7.9
Prism	49	7.5
2 × Prism 49	100	7.1
Grism	278	5.8
Grism	981	5.1
Grism	1724	4.8

Note: Reported magnitudes describe the estimated fringe tracking limit of MYSTIC under good atmospheric seeing conditions for a spatially resolved target. If fringe tracking can be accomplished exclusively with MIRC-X, it is possible to observe fainter targets with MYSTIC. Use of the  $R = 20$  prism is only supported for  $\leq 5$ -telescope observations in AIO mode due to cross-talk.

within its optical train. Since these actuators have neither the speed nor precision to maintain phase delay for the secondary instrument, the recorded fringe contrast does suffer some corruption resulting in higher uncertainties in the final reduced square visibilities. To somewhat mitigate this result, we have implemented a combined fringe tracking mode whereby both instruments inform the CHARA delay lines of their preferred offsets and a weighted average is used to approximate phase tracking across the two bandpasses; in general under this mode, neither instrument's fringe contrasts are optimal, but neither do the final reduced visibilities have as large uncertainties as they would have had were the other instrument acting as "primary."

Altogether, MYSTIC as-built satisfies all of the technical requirements enumerated in Sec. 3, though work is still ongoing to provide full software support for the ABCD combiner. Additionally, the instrument is currently fully equipped for the science cases driving its design, with the notable exception of emission line observations with either MIRC-X or MYSTIC. This too is largely a matter of software optimization, enabling ultra-stable fringe tracking with the aid of the counterpart instrument at low spectral resolution, which will require scheduling future dedicated facility engineering time to complete.

## 5 Warm Optics

The warm optics serve to extract the K-band light coming in from the six collimated CHARA infrared beams, to correct for group delay and differential birefringence between the beams, and to inject the light into fiber optics which feed into the cold optic subsystem. This system was designed to use as many off-the-shelf parts as possible, to be as easily accessible for alignment and maintenance, and to share space on an 8 ft.  $\times$  5 ft. optical bench with the MIRC-X instrument. Each component of the warm optics system is described in the following sections.

Care was taken to design the system with as few reflections as possible while also fully motorizing all necessary components to enable remote operation by observers. These two goals proved difficult to satisfy simultaneously while also offering two beam combiner modes, so two additional reflections were introduced into the beam path for the ABCD mode; more information is given in Sec. 5.5.

### 5.1 Dichroics

The first optic on the MIRC-X/MYSTIC table encountered by each of the CHARA infrared beams is a plane-parallel 2-in. dichroic, manufactured by Brinell Vision. The dichroics are placed at a 45 deg angle of incidence, and reflect K-band light into the MYSTIC optical train, while allowing the H-band light to pass through to MIRC-X at  $\geq 90\%$  efficiency across the bandpass. The incident surface of the 8-mm thick IR-grade Infrasil optic has the dichroic coating, and the emergent surface has an anti-reflective coating applied. The dichroics are mounted in optical holders (Thorlabs) all affixed to a single aluminum plate. Each of these optical mounts has two piezo rotary actuators (Newport Picomotors) for tip/tilt adjustment of the dichroics. These were used for initial alignment of the system, but since the alignment has remained stable, we anticipate rarely needing to use them in the future. The aluminum interface plate is attached to a Newport translation stage driven by a R256 stepper motor (Lin Engineering), enabling the dichroic assembly to be removed from the infrared beam-path for use by other instruments at CHARA (such as CLASSIC/CLIMB<sup>15</sup>). The 29.7 mm normal separation between neighboring dichroic mounts provides ample clearance for the 19 mm infrared beams to bypass MYSTIC unvignetted. For positional repeatability, a fixed photointerrupter is employed as a home switch for when the dichroics are inserted into the beams, triggered by a protruding piece of aluminum affixed to the linear stage.

### 5.2 Polarization Control

Differential phase shifts between the horizontal and vertical basis states of light are introduced by mirror reflections in the optical trains of CHARA and MYSTIC as well as birefringence in the optical fibers connecting the warm and cold optical subsystems (see Sec. 5.7), leading to loss in fringe visibility upon beam combination. We include a set of 4-mm thick, z-cut lithium niobate plates ( $\text{LiNbO}_3$ ), custom fabricated by Crylight Photonics, in the beam path. This follows a similar implementation to the one first used in the VLT/PIONIER instrument,<sup>16</sup> albeit with

a different crystal orientation. Birefringence control is then attained by rotating the plates relative to each other, effectively increasing the projected thickness of the material. In the K-band, these provide an adjustable phase shift of up to 5 beat lengths of differential OPD, while providing >99% transmission across the bandpass for incidence angles up to 30 deg.

Duplicating the design of the MIRC-X instrument, the lithium niobate plates are mounted on rotary stages (OES) with a resolution of 0.02 deg. Each axis is controlled by an R256 stepper motor (Lin Engineering) and is set with a home position oriented normal to the incoming beams. For regular operation, the plates are set to a nominal position of 20 deg and then are optimized for optimal fringe contrast using the internal light source. This operation consists of fixing the orientation of a reference beam's plate (typically CHARA beam 4) while slowly rotating the other plates and measuring the visibility of each beam with the reference. Non-reference plates are finally set to the maximum contrast positions. Commissioning results show that the plate positions determined using the internal light source conform well to the sky, despite the non-common path with nearly all of the array optics upstream of the MIRC-X/MYSTIC bench.

### 5.3 Differential OPD Correction

To maintain the mutual group delay between MIRC-X and MYSTIC, the next set of 1 in. gold fold mirrors are motorized for differential OPD correction. Adopting the differential delay line apparatus of the MIRC-X instrument, the mirrors are translated on linear stages (Newport) driven by precision linear actuators (Zaber) with a total travel range of 1 in. and a step size of 1  $\mu\text{m}$ , with better than 4  $\mu\text{m}$  repeatability. This facilitates adjustments on the order of 1 wavelength in position for coarse group delay adjustments but is not precise enough to maintain continuous phase referencing. Unlike their MIRC-X counterparts, these mirrors are fixed to unmotorized kinematic mounts (Thorlabs); alignment was fine-tuned and fixed during instrument commissioning.

### 5.4 Tip/Tilt Correction

Beam guidance for the CHARA Array is conducted at visible wavelengths, several reflections upstream of the instrument benches. Atmospheric differential refraction causes the beams to drift in the infrared over timescales of several minutes and over angular scales as high as 1 arcsec.<sup>17</sup> To maximize flux injection into the cold optic system, this tip/tilt error must be corrected as often as possible while minimizing operational overhead. MYSTIC employs a magnetic coil-driven fast-steering mirror (Optics in Motion) for each beam, with a  $\pm 3$  deg angular range and 0.25 arcsec resolution, corresponding to a tip/tilt correction of  $\sim 10$  mas on-sky. This provides ample steering resolution compared to the  $\sim 0.5$  arc sec diffraction limit of a 1-m telescope at K band.

The fast-steering mirror (FSM) modules themselves are 1.6 in wide, allowing the light traveling from the polarization control to the OPD correction optics to pass between them unvignetted. We created custom, 3D-printed mounts to affix unprotected gold mirrors to the magnetic coil drivers; the original mirrors were glued into the FSM assemblies resulting in unacceptably high wavefront errors due to the epoxy stress. A new hardware server was added to the MIRC-X/MYSTIC operational software (Sec. 8) to control the FSM hardware, which are steered by applying a voltage in the  $\pm 10$  V range along each of their axes. The new server communicates with a T7 series LabJack to apply and log the required voltages.

Use of FSMs provides some advantages over the fiber injection strategy employed by the MIRC-X instrument, where each fiber tip is placed on an XYZ motorized translation stage and moved to accommodate a drifting focal point. Since the optical fibers do not move in the MYSTIC design, there is less opportunity for variation in the stress birefringence of the fiber, providing stable polarization control. Moreover, since adjustment of the FSM angle occurs nearly instantaneously (<20 ms including communication overhead), scanning for the incoming flux angle is quicker than in the MIRC-X instrument where the fiber injection motors need time to arrive to position. That said, we do note a few disadvantages as well. Most notably, the FSM motor controllers produce a non-trivial amount of heat, causing the plastic housing to begin to melt if left on for extended periods of time. Since space constraints require the controllers for all six FSMs to be in very close proximity to each other and other electronics above the MIRC-X/MYSTIC table, they are powered down during daylight hours to prevent damage. Additionally, the FSMs require continuous power delivery to maintain their positions and need to be realigned after each power cycle. On rare occasions, we have also noticed sudden drifts in the mirror

positions; we have not yet isolated whether the mirrors, voltage source, or controllers are the root cause of this issue.

### 5.5 Periscope

Two additional 45 deg reflections in a vertical periscope arrangement intercept the light up toward a dedicated set of fiber injection modules when the ABCD combiner is in use. The lower set of gold-coated wedge mirrors are mounted to a common horizontal linear translation stage (Newport), driven by a R256 stepper motor (Lin Engineering), with motion perpendicular to the light propagation direction. When the lower periscope mirrors are removed from the beams, the light travels directly toward the fiber injection modules feeding the AIO combiner.

### 5.6 Fiber Injection

Each collimated light beam is focused onto the tip of a fiber optic by an off-axis parabolic (OAP) mirror (fibers are described in Sec. 5.7). The final assembly of the warm optic system is comprised of an interface plate securing the mirror, one end of the optical fiber, and the respective retaining optomechanics for each beam (see Fig. 4 for a schematic overview). A total of ten of these injection modules are installed in MYSTIC (six for AIO mode and four for ABCD mode).

The assemblies were designed to accommodate off-the-shelf OAP mirrors in a configuration that met the acceptance cone of the fiber optic without the fiber or its mount obstructing the neighboring light beam. For this task, we chose a gold-coated mirror (Edmund Optics) with a 30 deg reflection and an effective focal length of 54.45 mm but found that the mirrors we procured induced significant coma aberration at the optimal image quality alignment for our setup. We ultimately ordered a set of custom diamond-turned OAPs with the same dimensional specifications and a surface figure of  $< \lambda/20$  RMS at 632.8 nm (delivered by Nu-Tek Precision Optical Corp.). The custom mirrors do not exhibit low order aberrations and focus the light onto a smaller spot compared to the stock mirrors; Fig. 5 compares the optimal image quality of the two mirror batches.

The fibers are connected via an FC connector to an L-bracket placed on a manually operated translating stage (Newport) which provided focus adjustments during initial alignment of the system. The OAPs are secured by kinematic optical mounts (Newport) with two degrees of freedom for tip/tilt adjustment. Image quality optimization of each injection module was completed by back-projecting visible laser light through the fiber optic while adjusting the tip/tilt and rotational orientation of the mirror until the smallest spot size of the reimaged emergent collimated beam was obtained. Upon alignment, the tip/tilt adjustments were locked in place. Individual injection modules for each combiner mode were mounted together on a single plate; AIO mode injection modules hang on the underside of one interface plate and the ABCD mode modules are

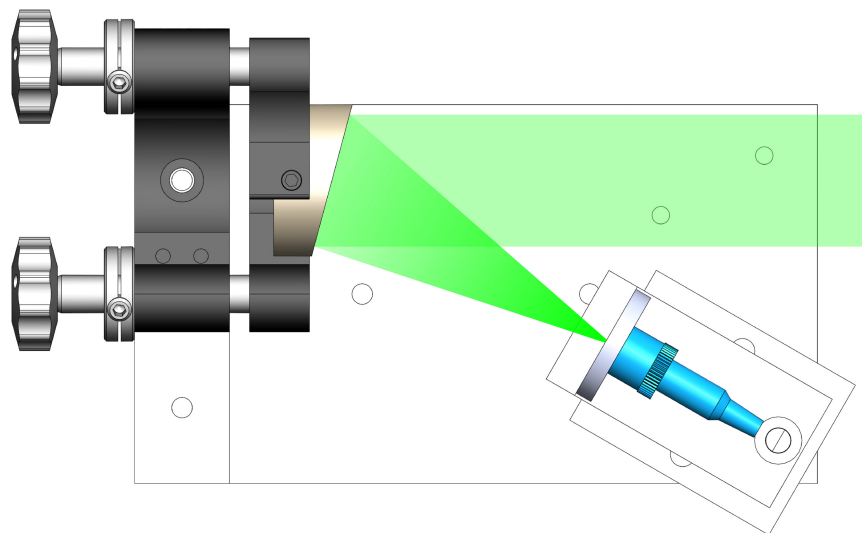


**Fig. 4** Schematic view of the fiber injection mount. CHARA beams are reflected by a gold-coated off-axis parabolic mirror and focused onto a fiber tip.

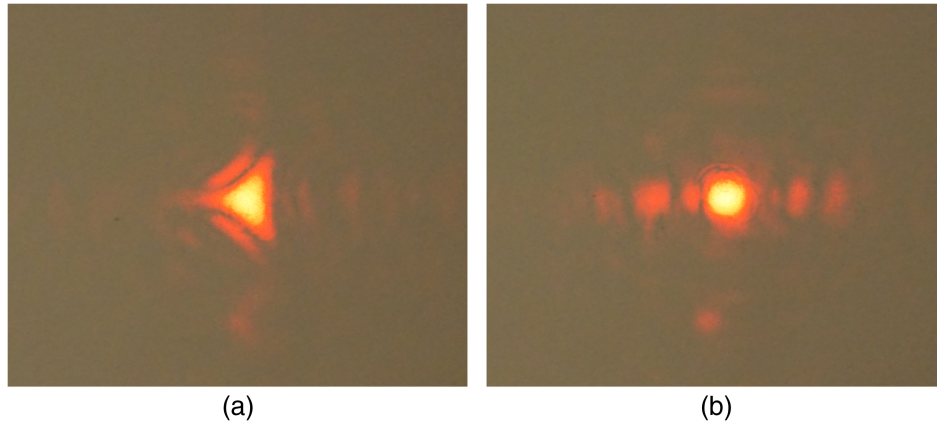


**Fig. 5** A HeNe laser signal is emitted from a fiber optic at the focal point of each OAP; the images above show the resulting collimated beam refocused by (a) an off-the-shelf OAP mirror produced by Edmund (Stock #35-491) and (b) a custom fabricated OAP by Nu-Tek. The former produces a strong coma, whereas the latter produces a smaller overall spot and does not display significant low order aberration. Both images are shown at the same physical scale.

placed on top of a second plate above. Coalignment of the injection modules to the collimated MYSTIC beams was accomplished with judicious use of plastic shim stock.

### 5.7 Fiber Optics

Optical fibers are employed in MYSTIC to transmit light from the lab into the cryogenic dewar. Altogether, each participating CHARA beam is transported through three connected fibers: first via a patch cable linking the injection module to an external plug-plate, then through a vacuum sealed feedthrough tube traversing the cryogenic dewar wall to an internal plug-plate, and then finally either via a fiber glued into the AIO V-groove module (see Sec. 7.1) or the ABCD optical chip (see Sec. 7.2). A three fiber train was chosen instead of a simpler one or two fiber system to facilitate better overall length-matching and to prevent accidental breakage of the feedthrough fibers during testing, despite a greater injection loss due to the additional coupling.

The fibers were selected to be single-mode,<sup>18</sup> acting as a spatial filter removing non-zero photon orbital angular momentum modes introduced into the wavefront signal by atmospheric turbulence, and polarization maintaining, to ensure temporally stable fringe contrast between the horizontal and vertical polarization modes as measured by the detector. Furthermore, the chosen fiber was required to accommodate the ABCD combiner chip with a numerical aperture of 0.19. After internally testing several off-the-shelf optical fibers, Nufern PM1950 silica-based fibers were selected for use in MYSTIC as they provide a high throughput throughout K-band, suffering low OH absorption at longer wavelengths. Table 2 summarizes measured properties of these fibers. Compared to the fluoride-glass fibers used in the GRAVITY instrument, PM1950 fibers were more cost effective and less delicate than their counterparts.

**Table 2** Properties of Nufern PM1950 silica fibers.

Property	Value
Core NA	0.2
Cutoff wavelength	1.72 $\mu\text{m}$
Mode field diameter at 1.95 $\mu\text{m}$	8.0 $\mu\text{m}$
Core diameter	7 $\mu\text{m}$
Beat length at 1.95 $\mu\text{m}$	5.2 mm
Throughput/meter at 2.2 $\mu\text{m}$	94%
Throughput/meter at 2.37 $\mu\text{m}$	85%

To mitigate visibility loss due to differential dispersion between fiber trains, each fiber set was cut and connectorised to a consistent length (Costal Connections). The lengths of all available fibers were measured using an optical backscatter reflectometer (Luna), with typical fibers in each set matched within 0.5 mm. The optimal combinations of fibers for each train was determined to minimize the total length difference, thus minimizing chromatic dispersion. For the AIO combiner, the longest train exceeds the shortest by a length of 73  $\mu\text{m}$ , with a typical difference between trains of 23  $\mu\text{m}$ . For the ABCD combiner, the greatest difference is 2.12 mm with a typical difference of 0.87 mm. (A second spare ABCD combiner from VLTI/GRAVITY was also prepared with a fiber V-groove—see Sec. 7.2—which could have been matched with a greatest difference in total fiber length of 35  $\mu\text{m}$  and a typical difference of 14  $\mu\text{m}$ . However, due to a miscommunication within our team, the significantly less ideal chip had the microlens array glued to it in preparation for MYSTIC. We will consider replacing the currently installed ABCD combiner at a future date.)

Separate vacuum feedthrough sets were created (Costal Connections) for the two beam combiners, each with a total of nine length-matched, connectorised PM1950 fibers vacuum sealed with an epoxy. The extra cables provided more flexibility in choosing optimal fiber combinations for each beam. We commend the consistency in the final lengths Costal Connections were generally able to achieve for these fibers, though we ultimately had to purchase a third fiber feedthrough set as the first one we received was improperly sealed and unable to maintain vacuum integrity at  $10^{-6}$  mbar.

Except for the final glued connection, each fiber end is terminated by an FC/PC connector. After cleaning the fiber tips, a typical 5% to 10% throughput loss at each connection could be achieved, with the net throughput varying within this range each time cables were unconnected and reconnected together. Overall, we measured average throughputs across K-band ranging between 60% to 80% among all employed sets of patch cable and vacuum feedthrough cable, with a total average fiber length of 101.0 cm for the AIO mode fiber pairs and 98.5 cm for the ABCD mode fibers. We found that the FC/PC connectors designed for vacuum applications, with a hexagonal shaped thumb screw, could be connected and disconnected with ease in tight spaces, while mitigating risk of damaging the fibers, with the aid of a flare nut socket.

## 6 Cryogenic Dewar

Interferometric beam combination occurs within a custom rectangular cryogenic vacuum dewar (Universal Cryogenics) to minimize the contribution of thermal background from the lab in the K-band upon fringe measurement. The cold optic system (see Sec. 7) is placed within the cryostat atop a  $15 \times 13$  in. optical breadboard. The space between the outer and inner wall of the dewar is filled with several layers of superinsulation (MLI) to reduce the thermal load on the cooling system. The dewar includes the following interfaces: two 2.75 in. ports for the fiber-optic feedthroughs, a DN100 port for the externally mounted C-RED One camera, two external stepper motors driving the internal filter wheel (see Sec. 7.3) via a ferrofluid interface, an electronic feedthrough, a vacuum feedthrough, and hose connections for the cooling system. Access to the inside of the dewar is facilitated by a removable lid. Figure 6 shows an inside view of the cryostat.

While in operation, the dewar is maintained at a pressure of roughly  $6 \times 10^{-6}$  mbar. The vacuum is provided by a turbo pump. The initial pump-down from atmospheric pressure typically completes over the course of several hours, but may take up to a few days if the dewar has been at atmosphere for an extended period of time. (We believe this is primarily due to the slow out-gassing of air trapped within the superinsulation layer. If we were to design the instrument again, we would opt for several layers of aluminum plate between the inner and outer walls of the cryostat instead.) Like MIRC-X, MYSTIC's vacuum systems are equipped with electromagnetic valves which close during a power outage and must be manually reopened.

Once the internal pressure of the dewar reaches  $10^{-3}$  mbar, the cryostat is cooled by a Polycold Compact Cooler (Brooks Automation) with Standard grade NF-55 refrigerant. Since this fluid would continue to cool the system to 183 K, far lower than our specifications demand, a small heater is placed inside the dewar to actively maintain an operating temperature

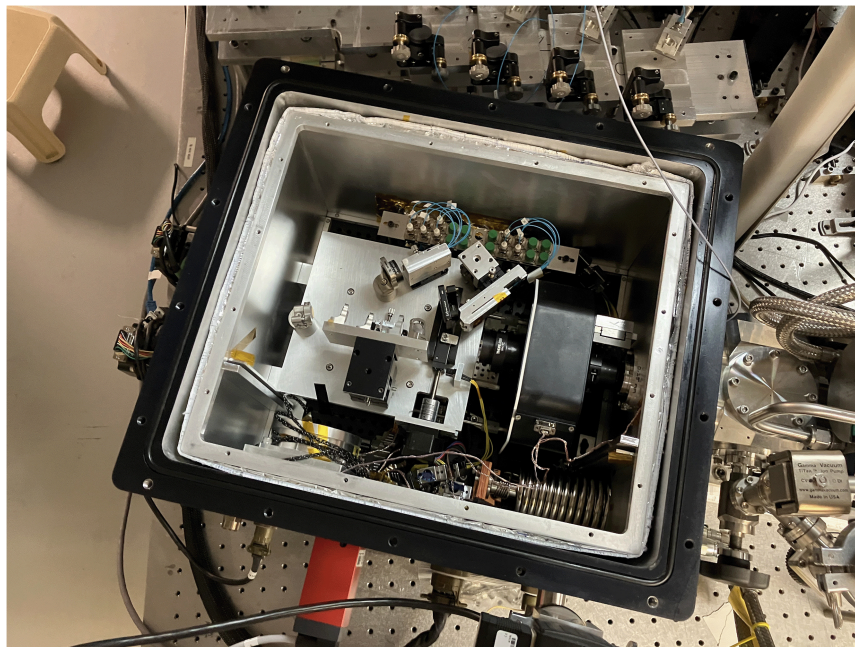


**Fig. 6** An inside view of the MYSTIC dewar (note that the aluminum sheet which blocks thermal photons emitted directly from the heater is removed). Inside the dewar: at the top is a fiber plug plate with the vacuum feedthrough fibers connected on the underside. The group of fibers to the left connect to the AIO V-groove where the light is then reflected into the AIO combiner immediately below. The group of fibers on the right connect directly to the ABCD combiner. Immediately following the ABCD combiner is the translating mirror which determines which combiner's light proceeds toward the camera. To the right is the filter wheel, with collimating and focusing optics before and after, respectively. The filter wheel is attached to two rods along the base (not visible) connected to external motors for rotating the optics. On the lower right is the cooling coil; a heating element is placed on the dewar base (not visible). Outside the dewar: at the top are the two fiber feedthroughs (not visible). On the right is the C-RED one camera. At the bottom right is the vacuum pump connection, and the red element near bottom center is the pressure gauge. On the left side are the filter wheel stepper motors.

of 220 K. An aluminum shield is placed between the optical elements and the cooling coils and heater in order to prevent stray reflections of the K band light emanating from the thermal head from coupling into the beam path. Two thermometers are placed on the optic side of the aluminum shield, which inform a PID loop controlling the thermal head via an external temperature controller (LakeShore). In case of a thermal head failure, the temperature controller sends a signal to turn off the cooling compressor if the temperature drops below 219 K. The thermal head is also used when cooling the system from room temperature; to prevent thermal shock of the internal components, the dewar is cooled at a rate of 0.034 K/min, which brings the cryostat to temperature over the course of 48 hours.

Between the inner dewar wall and the C-RED One camera window, we inserted a baffle tube comprised of a series of traps (flat rings) of varying inner diameters in an attempt to minimize stray thermal background light from coupling into the beam path (see Fig. 7). Each of these disks were coated with an application of Singularity Black paint (NanoLab) to maximize light absorption. Although this did help in significantly reducing the total thermal background measured by the detector, we nevertheless report a 2.4 times higher median flux per pixel than anticipated (typical 360 ADU/s, compared to an anticipated 150 ADU/s at an operating camera gain of 40). We have concluded that the dominant source of background flux is not coming from within the MYSTIC cryostat but instead is scattering into the C-RED dewar through the sapphire window separating the camera and MYSTIC dewar. The window is not entirely optically isolated from the lab (see Figs. 7 and 8). We will explore avenues to reduce this flux in the future, such as operating without the window entirely (see Sec. 10).

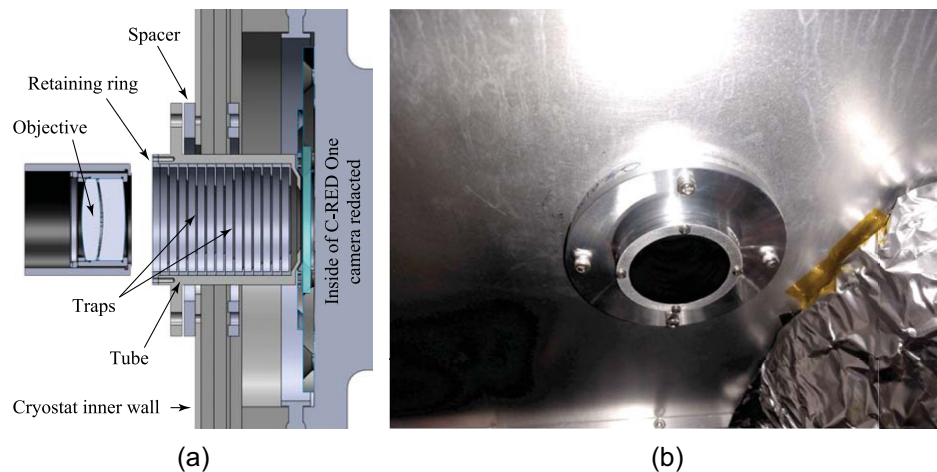


**Fig. 7** (a) Position and schematic cut view of the baffle tube assembly and (b) an image of the baffle tube mounted on the inner wall of the MYSTIC cryostat. The baffle tube consists of a series of varying inner-diameter traps coated in Singularity Black paint, which absorb stray thermal background light.

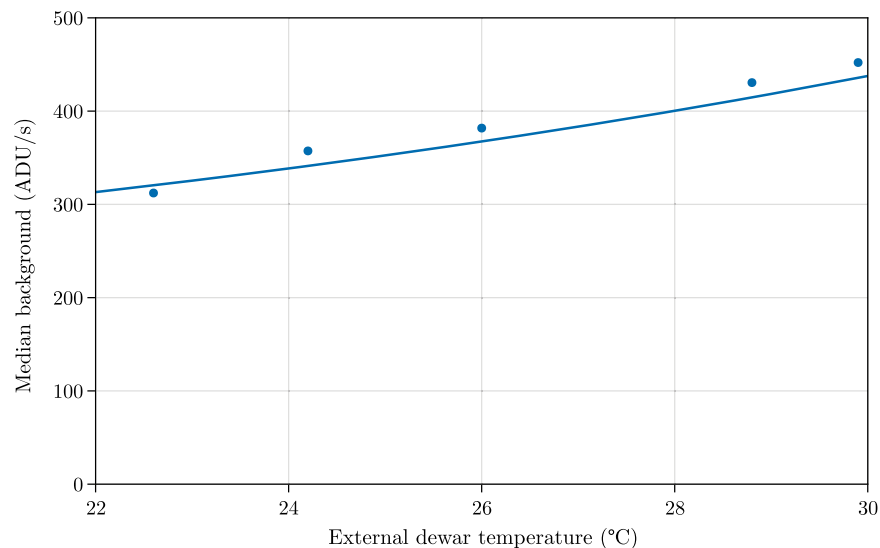


**Fig. 8** Median pixel count of the background with the detector set to a Gain of 40. By heating the external case of the dewar, we see additional thermal light coupling into the detector. The roughly fit line illustrates blackbody thermal light coupling into the camera chamber in excess of a 150 ADU/s background.

## 7 Cold Optics

The cold optics system consists of the beam combiners and spectral dispersing elements, together with a couple motorized optics necessary for aligning the dispersed light onto the detector. Each of these elements, together with the C-RED One camera, are described in the following sections. A schematic drawing of the optical elements in the cold optics system is presented in Fig. 9.

The cold optic system includes four stepper motors and translation stages inside the cryostat. We found that, after removing grease from the internal bearings of these elements, they work just fine at cryogenic temperatures, bypassing the need to purchase components specifically advertised and priced for cryogenic applications. In lieu of grease lubricating our linear translation stage bearings, we applied a layer of MoS<sub>2</sub> powder to facilitate smooth motion. Operation of these elements was successfully tested inside a cooler filled with dry ice (198 K) before being added to the dewar.

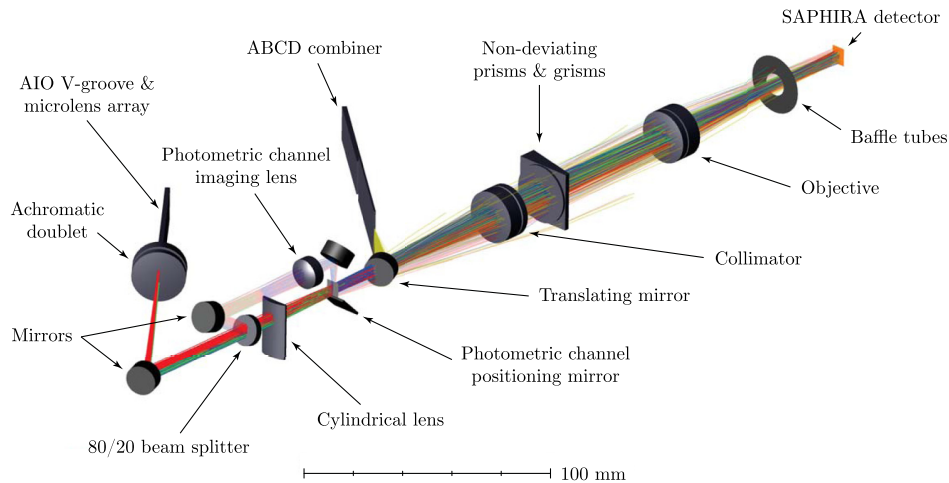


**Fig. 9** Annotated layout of the cold optic system, with beam trains for both combiners overlaid. To the left of the translating mirror are the AIO mode optics. This mirror slides out of the beam train for AIO mode observations or into the beam train for ABCD mode observations.

### 7.1 All-in-One Beam Combiner

The AIO beam combiner borrows heavily from the design of the MIRC-X combiner. Herein, we provide a brief description of the combiner, particularly highlighting differences between the MYSTIC version to that of MIRC-X. We note that this design is cross-talk resistant if observing with 5 or fewer telescopes. For a more in-depth discussion on the design of the AIO combiner, we refer the reader to Ref. 8.

Fiber optics carrying light from each of the six CHARA beams are arranged vertically in a non-redundant spacing on a silicon V-groove (OZ Optics), in slots 4, 6, 13, 18, 24, and 28 with a  $250\ \mu\text{m}$  pitch, providing a unique spatial frequency in the subsequently interfered light for each pair of beams. The fiber ends are glued to a microlens array which collimates the fiber outputs. The microlens array was custom made (Mackinac MicroOptics) to accommodate the higher numerical aperture of the MYSTIC fibers compared to those in MIRC-X. The array consists of 48 fused silica parabolic lenses spaced in a single line  $250\ \mu\text{m}$  apart, with the diameter and radius of curvature of each lens also  $250\ \mu\text{m}$ , all on a  $0.729\ \text{mm}$  thick IR-grade fused silica substrate. These micro-lenses were then carefully aligned with a Fabry–Pérot interferogram and glued in place.

The collimated beams are then “focused” by a  $200\ \text{mm}$  focal length achromatic doublet (Thorlabs), yielding a highest frequency sampled at the detector of  $2.64\ \text{pixel/fringe}$  at  $1.9\ \mu\text{m}$ . As the beams converge, a reflection redirecting the light path is introduced, keeping the system within the constraint of the dewar, followed by a beamsplitter which extracts 20% of the light from each beam for subsequent photometric measurement. The remainder of the light continues through a cylindrical lens near the focal point, emulating a slit where the interference pattern is generated. The  $\text{CaF}_2$  cylindrical lens used here is repurposed from the original MIRC instrument, with a  $30\ \text{mm}$  focal length. Following the cylindrical lens, the previously extracted photometric light is reimaged and then directed via mirrors below and parallel to the primary ray of the interfered light where both pass on to the spectrograph collimator (Sec. 7.3). A typical detector image with the AIO mode in optical delay is shown in Fig. 10 with fringes from all 15 baselines overlaid on top of each other and with the photometry measurements beside. We note that there is an  $\sim 1$  pixel shift in the spectral direction between the fringes and the photometric channels due to small changes in alignment between room temperature and the dewar operating temperature at  $220\ \text{K}$ .

### 7.2 ABCD Beam Combiner

The ABCD combiner is a spare integrated optics chip produced for the GRAVITY instrument.<sup>13</sup> It conducts a four beam pairwise (six baseline pairs) ABCD combination whereby the fringe contrast for each baseline pair is sampled at four phases in quadrature, allowing the instantaneous

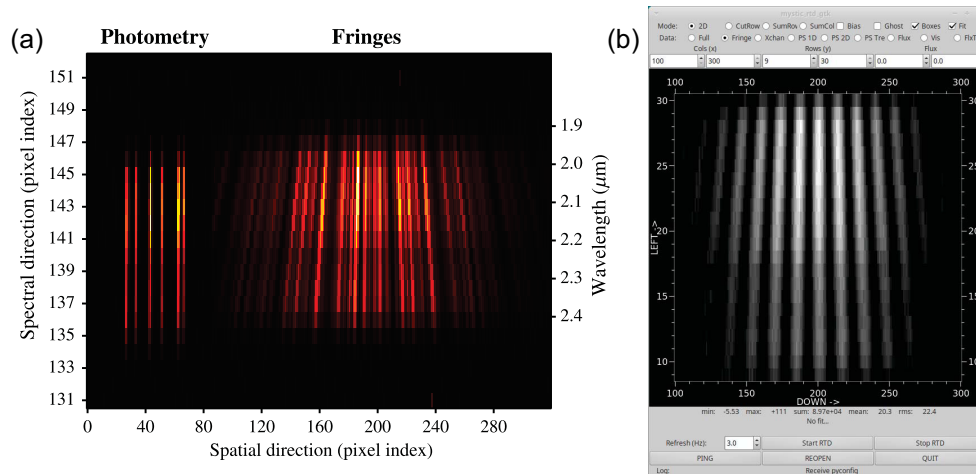


**Fig. 10** (a) A typical detector readout with six telescope delay in AIO mode. Photometry is measured at each wavelength channel on the left of the detector readout and interferometric fringes are formed on the right, with the fringes of all 15 baselines superimposed at non-redundant spatial frequencies. Note that due to a slight misalignment, the photometric channels are shifted  $\sim 1$  pixel in the spectral direction compared to the fringes. (b) An example of a fringe pattern with two beams only (beam 2 and beam 3).

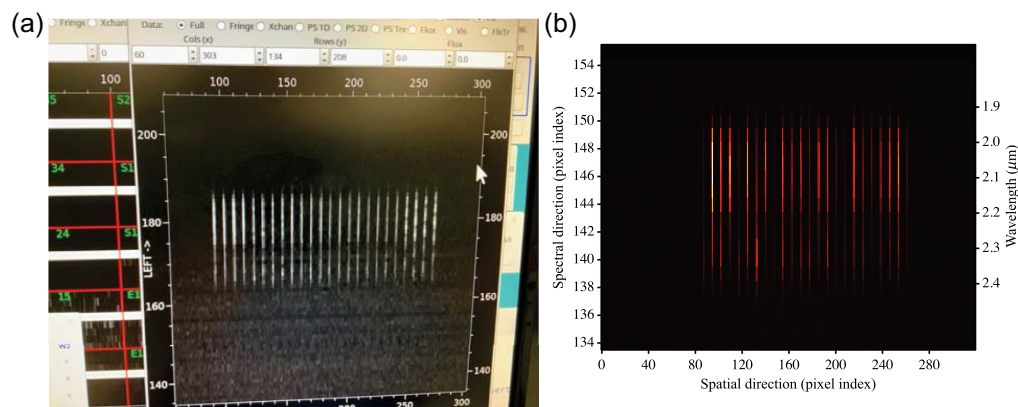


**Fig. 11** ABCD chip observations appear on the detector as a series of 24 parallel lines, measuring four phases of the visibility contrast at each wavelength channel. (a) Several outputs show regular light and dark bands along the spectral direction, indicating unoptimized optical path delay at the time this photo was taken. (b) The optical path delay is corrected and for each baseline, the ABCD outputs show varying flux intensity indicative of measured fringe contrast.

complex visibility to be measured. We refer the reader to Ref. 11 for a more in-depth discussion of the chip itself.

The chip's 24 outputs are separated by  $180 \mu\text{m}$  (7.5 pixels on the detector; see Fig. 11). A custom microlens array, consisting of 72 lenses, each with a diameter and spacing of  $180 \mu\text{m}$ , a radius of curvature of  $200 \mu\text{m}$ , and a thickness of  $0.450 \text{ mm}$ , was manufactured (Mackinac MicroOptics) on an IR-grade fused silica substrate to adapt the chip's output  $f$ -number from  $f/2$  to  $f/12$ . The microlens array and a set of PM1950 fibers arranged in a V-groove were affixed to the ABCD combiner chip with a UV polymerized glue (Epo-Tek OG142-87) onto a common mechanical support (see Fig. 12).

The final assembled beam combiner was mounted just behind the AIO combiner assembly. A 1 in. gold mirror, placed on a linear translation stage (Newport) and actuated by a Nema 14 stepper motor (Jkong Motor), is used to either reflect light from the ABCD chip into the optical path immediately before the spectrograph collimator, or allow light from the AIO combiner to pass through instead.

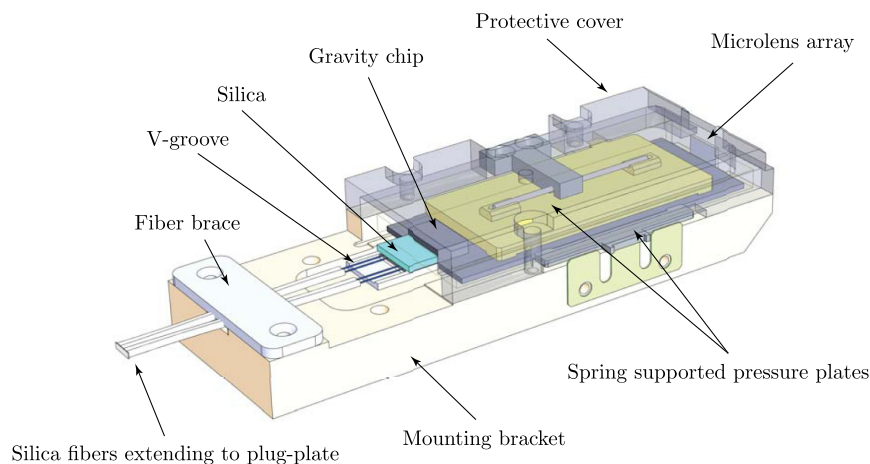


**Fig. 12** Schematic of the ABCD combiner assembly prepared at IPAG. Note that the cover protecting the GRAVITY chip from incidental damage is made transparent in this diagram for illustrative purposes only.

### 7.3 Spectrograph

Following the beam combiners, MYSTIC includes a spectrograph consisting of a collimating optic on an XZ linear stage (spectral and focal direction), two filter wheels—each with six slots—containing an assortment of dispersive optics, and an objective on a Y linear stage (spatial direction) which focuses the light onto the detector. We note that while having the focus adjustment on the collimator optic is not ideal, the Z location of the objective was carefully positioned for optimal focus at 220 K (determined via Zemax modeling of the system). Moving the collimator in the Z direction is necessary only during engineering tests when the inside of dewar is at lab temperature.

The collimator and objective are off-the-shelf achromatic doublets (Thorlabs ACA254-100-D), mounted inside Thorlabs SM1 tubes, attached to motorized linear stages (Newport), and driven by Nema 14 stepper motors (Jkong Motor) connected to the stage via an aluminum beam coupling (Ruland). Under cryogenic conditions, we notice significant hysteresis in our modified stages, whereby the light positions in the detector typically drift by a pixel after moving the stages a millimeter and then back. Moreover, since the X stage sits atop the Z stage, motions in the latter affect the position of the former on about a 1 pixel level.

The two filter wheels are joined together as a single assembly. Rotation of the wheels is facilitated by external DC stepper motors connected to the wheels via shafts along the base cold-plate of the dewar. The wheels are configured in a 6:1 gear ratio, so a single revolution of the connecting shaft advances a filter wheel by one position. A notch with a spring loaded homing switch marks the position of one of the slots in each wheel. The first wheel has a depth of 15 mm and the second has a depth of 29 mm. Each slot is designed to accommodate a 1 in. square optic or a 1 in. circular optic mounted inside an SM1 tube (which were cut to length on a lathe). Square optics are held in place by small, thin beryllium copper tabs.

The optical elements filling the wheel slots are enumerated in Table 3. The cold plug consists of Singular Velvet Appliqué (NanoLab) affixed to an aluminum puck and was used as a thermal background reference. The gratings are all custom 1 in. diameter Schott IRG7 wedges (United Crystals Inc.), with plane ruled transmission gratings adhered to the wedge surface (Richardson Gratings; the gratings were selected from Richardson’s standard catalog). We note that half of the originally delivered gratings suffered from severe grating alignment errors and were subsequently remade. The gratings were mounted inside of Thorlabs SM1 tubes with a cylindrical aluminum shell cut to a matching wedge angle, painted with Singularity Black and placed inside the SM1 tubes to prevent the gratings from toppling over as the wheel rotates. The gratings are held in place by a silicone o-ring spacer (Marco Rubber) and an SM1 retaining ring. The Wollaston prism (United Crystals) is a square optic made of two perpendicularly oriented quartz wedges optically cemented together, producing a  $\sim 1$  deg splitting angle. Since the delivered Wollaston prism was marginally thicker than the depth of the first filter wheel, we 3D printed a 2 mm spacer for the wheel backplate to accommodate the optic.

**Table 3** Filter wheel elements.

Slot	Wheel 1	Wheel 2
1	Empty	Empty
2	Cold plug	$R = 20$ prism
3	$R = 278$ grism	$R = 49$ prism
4	$R = 49$ prism	Empty
5	Narrow band filter ( $1.930 \mu\text{m}$ )	$R = 981$ grism
6	Wollaston prism	$R = 1724$ grism

Several non-deviating prism pairs were custom fabricated (United Crystals), with spectral resolutions  $R$  of 20, 49, and 100. Each prism was made with an Infrasil glass wedge followed by a  $\text{CaF}_2$  wedge. In the first iteration of prisms, the optics were square with optical cement holding the wedges together. Upon testing these optics under cryogenic conditions, the  $\text{CaF}_2$  halves shattered; believing this was caused by tight mounting inside the filter wheel imposing stresses on the optics during thermal contraction, we ordered a second set of circular prisms to be mounted inside SM1 tubes instead. Again, upon cooling, the  $\text{CaF}_2$  halves shattered. Eventually, we identified that differential thermal contraction between the Infrasil and  $\text{CaF}_2$  halves at 220 K produced shear stress on the Calcium Fluoride crystal beyond its fracture limit. We commissioned a third set of prisms with wedges cut to specification but not optically cemented them together and we 3D printed thin spacers to place between the wedge halves before mounting into the filter wheel slots. Unfortunately, with an air gap between the strong wedge angles in the  $R = 100$  prism, the Infrasil optic exhibited total internal reflection. To recover this spectral mode, we ordered a second  $R = 49$  prism pair so as to place one pair in each wheel. Ray-tracing predictions of the light passing through both prisms in succession yields an expected final spectral resolution of  $R = 99.5$ .

#### 7.4 Detector

At the end of the optical train, a First Light C-RED One camera<sup>19</sup> is externally attached to the dewar wall. Featuring a  $320 \times 256$  pixel Leonardo SAPHIRA detector<sup>6</sup> with a  $24 \mu\text{m}$  pixel width, operating at a high vacuum of  $10^{-7}$  mbar and at 80 K, the camera delivers full-frame readout rates of 3.5 kHz with sub-electron read noise per pixel. Often, only a subset of the full frame is read for typical science configurations, further increasing the raw frame rate. Several readouts are then averaged per frame,<sup>8</sup> reducing the noise further and setting an operational frame rate typically closer to 400 Hz. During an observation, many frames are subsequently readout non-destructively before the pixels are reset.

The vacuum pressure is started by a turbo-pump shared by MIRC-X and MYSTIC cameras and then isolated and maintained by a dedicated ion pump (Gamma Vacuum). The camera is cooled using an internal pulse-tube cryocooler operating at 47 Hz with two coolant hoses connected to an external water chiller maintained at  $10^\circ\text{C}$ . A low-amplitude ( $\sim 20$  ADU/s RMS) 94 Hz nuisance oscillation is present in the detector readout related to the pulse-tube operation; this C-RED One was one of the earliest units produced by First Light and newer units have this issue fixed.

Immediately behind a sapphire window isolating the MYSTIC cryostat from the camera's internal vacuum system are three filters that prevent thermal background photons outside of the science bandpass from entering the detector chamber. The first of these filters is custom produced by Brinell Vision and sets the overall bandpass for MYSTIC, yielding  $>90\%$  transmission for 1.98 to  $2.36 \mu\text{m}$  and  $<1\%$  transmission outside the range 1.81 to  $2.51 \mu\text{m}$ . Figure 13 reports the measured throughput of this filter. The remaining two filters were provided by First Light and prevent photons with wavelengths exceeding  $2.45 \mu\text{m}$  from reaching the detector.

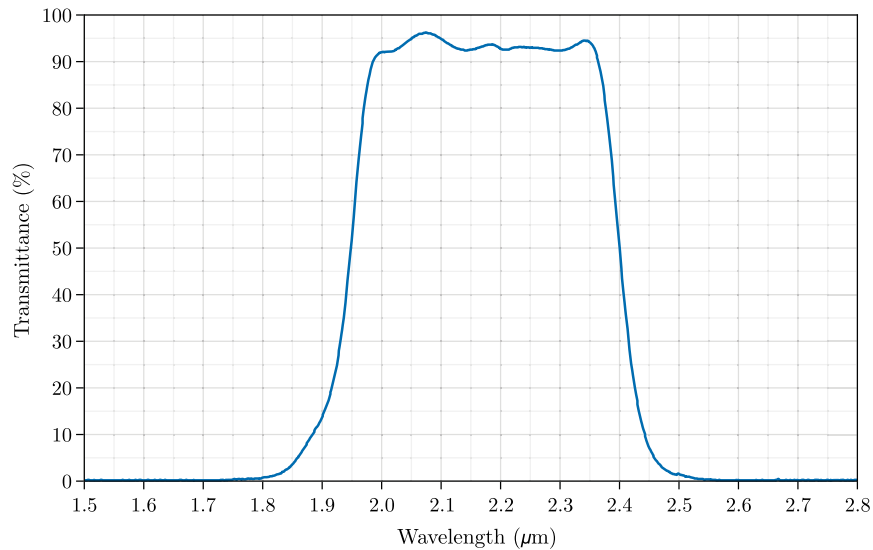


**Fig. 13** Measured throughput of the custom K-short bandpass filter inside the CRED-One camera, produced by Brinell Vision. This was added to reduce the thermal background measured on the detector (see Sec. 6).

## 8 Software Architecture

The instrument operational software was designed from its conception to provide the same interface for controlling MIRC-X and MYSTIC. Both instruments operate on a client/server model, allowing any number of GUIs, either on-site or remotely, to connect to servers running at CHARA. Although the MYSTIC camera interface and data acquisition is handled by a separate computer to that of MIRC-X, many other servers of the MIRC-X instrument are extended to now include MYSTIC subsystems in a single GUI. For example, the stepper motor server communicates with all DC stepper motors on the entire MIRC-X/MYSTIC table and the vacuum server now monitors the internal temperatures and pressures for both C-RED One cameras and the MYSTIC dewar. Figure 14 shows a simplified model of the server interconnections between MIRC-X and MYSTIC. We direct the reader to Ref. 8 for a thorough overview of the software implementation.

With the installation of MYSTIC, we have placed four, single-axis piezoelectric accelerometers (Brüel & Kjær) on the combined MIRC-X/MYSTIC optical bench to measure vibrations in the system, which are a potential cause for fringe contrast drops. These accelerometers are monitored and logged by the shared vacuum server, with RMS vibration measurements included in data file headers over the course of a file integration.

The super server, which manages data sequencing and provides a high level interface to other hardware servers to configure instruments for observing and communicating with CHARA servers, has been updated to allow for simultaneous data collection in both instruments. In addition to data, background, foreground, and shutters frames, the super server additionally implements a new sky frame mode. For MIRC-X, it is sufficient to close internal shutters, blocking the CHARA beams from reaching the detector, to estimate the background contribution. However, for MYSTIC, the shutters themselves contribute to the thermal background and are thus unsuitable for data calibration. In this mode, the server requests an offset off of the target to the telescope control loops to prevent a bias in the background measurement.

The most significant new feature involves simultaneous active group delay tracking of the MIRC-X and MYSTIC instruments together. Delay line control is implemented in two modes. In the first mode, the observer sets one instrument as the primary fringe tracker controlling the CHARA delay lines, with the second instrument adjusting its own independent differential delay lines. In the second mode, flux and contrast information from both instruments are used together to control the CHARA delay lines and internal corrections.

Since the AIO combiner mimics the MIRC-X design, and both MIRC-X and MYSTIC employ a C-RED One camera for data collection, minimal changes to the MIRC-X data

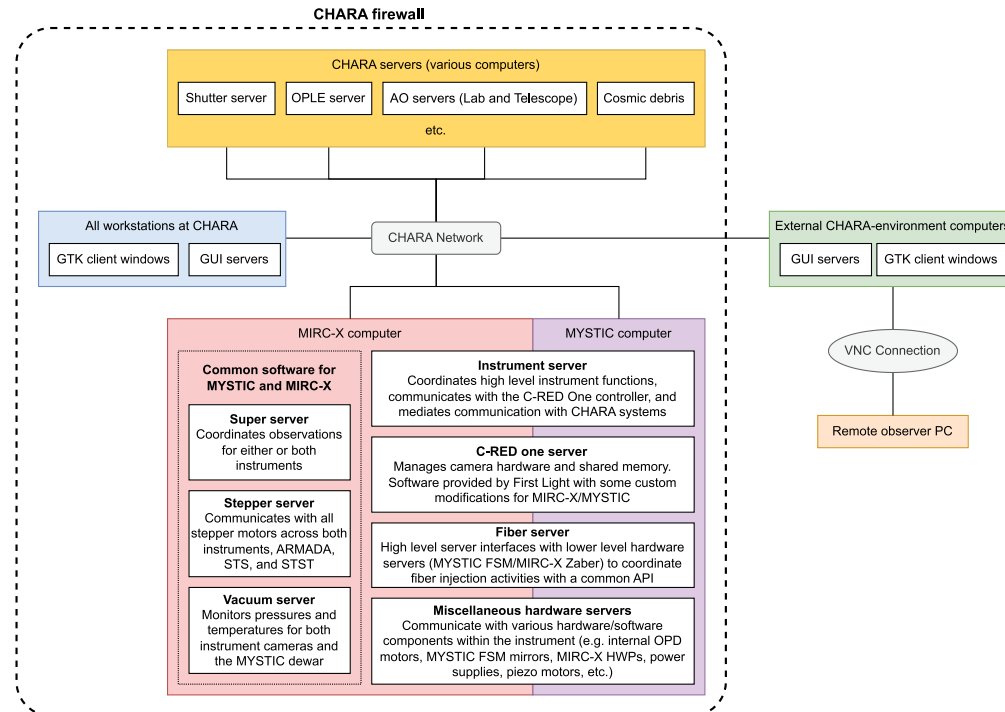


**Fig. 14** Simplified overview of the various software servers in MIRC-X/MYSTIC and their integration with other servers at CHARA. We note that while many servers related to the operation of hardware components unique to MIRC-X and MYSTIC run on their respective instrument computer, some additional servers related to shared hardware or the system as a whole operate on the MIRC-X computer (see left side of red box). GUIs operate on a client/server model whereby a single GUI server of each type connects to its respective instrument/system server(s) and then multiple GTK client windows then interface via the GUI server.

reduction pipeline were necessary to accommodate MYSTIC data in this mode. Most notable is the inclusion of sky frames used for background subtraction of the data. The ABCD mode observations are not yet supported by the pipeline. A substantial overhaul of the data reduction library is in progress both to support reduction of these data as well as to provide more manual control for bad header information correction and bad data rejection.

## 9 Instrument Performance

In this section, we examine early on-sky data of the well-known, 10.2 day period binary star system Iota Pegasi with MIRC-X and MYSTIC on September 15, 2021. These data were collected using all six CHARA telescopes, with the AIO combiner and an  $R = 50$  spectral resolution prism and the detector readout gain set to 20. These observations consisted of repeated pointings to the science target, interspersed with observations of several nearby calibrator objects (HD 207978, HD 214458, HD 213178, and HD 213026) to estimate the transfer function. Atmospheric seeing conditions varied throughout the night, with  $r_0$  values ranging from 8 to 12 cm. The adopted diameters of calibrator objects were based on theoretical predictions, provided in the JSDCv2 catalog.<sup>20</sup>

The data were reduced and calibrated with the MIRC-X pipeline, version v1.3.5-52. The data were separated into 5 min epochs and fit to a geometric model composed of two uniform disks with variable diameters, fluxes, and separation. Figure 15 shows a sample of these data points and the subsequent model fits. We find excellent agreement between the model and data closure phases. We find that the data reduction pipeline does not well calibrate the square visibility data at the shortest baseline, which is set to the lowest spatial frequency in the MYSTIC AIO combiner and includes crosstalk from the DC spike. These discrepancies will be improved in the near future with on-going developments to the data reduction pipeline.

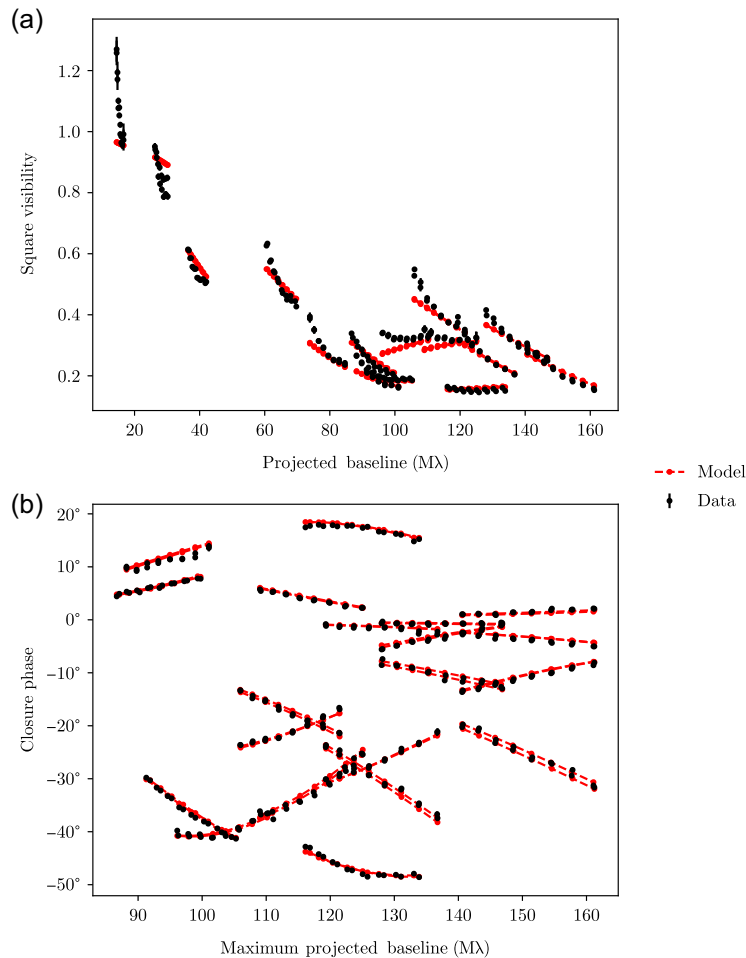


**Fig. 15** Sample MYSTIC data reduction and model fit to the binary star system  $\iota$  Peg. (b) Closure phases show excellent agreement with the model binary. (a) Square visibility measurements exhibit some miscalibration, especially at the shortest baseline, which will be addressed in future versions of the data reduction pipeline.

We verify the astrometric capability of MYSTIC by fitting for the orbital separation and flux ratios of the two stars while fixing their diameters to 1.05 and 0.60 mas for the primary and secondary, respectively.<sup>8</sup> We recover a K-band flux ratio of 4.45(14)—in rough agreement with Ref. 21 who report a K-band flux ratio of 4.677(65)—and show excellent agreement with the known orbit of the system (see Fig. 16). We note that for the earlier portion of the night, when contemporaneous MIRC-X data were recorded, the reduced MYSTIC data show a small systematic shift in position compared to MIRC-X, implying a small wavelength miscalibration for MYSTIC. We note that a meaningful estimate of systematic errors in astrometric precision can only be determined after many years of use. Such errors will be corrected for in future versions of the data reduction pipeline. Nominally, the astrometric performance is comparable to MIRC-X under similar observing conditions (see  $\iota$  Peg error ellipses in Fig. 16, right most panel).

After the necessary pipeline improvements are completed, we will revisit these  $\iota$  Peg data in an upcoming publication (Flores et al., in prep).

## 10 Concluding Remarks

MYSTIC is a science-ready instrument which meets its design goals for concurrent YSO observations with the MIRC-X combiner. Six beam solo fringe tracking has been demonstrated for objects as faint as  $K_{\text{mag}} = 7.7$  at an  $R = 50$  spectral resolution, and MYSTIC is able to co-track fringes with MIRC-X for observations of fainter objects. We report an  $\sim 3$  times higher thermal background than anticipated at the detector, lowering our overall sensitivity by 0.6 magnitudes,

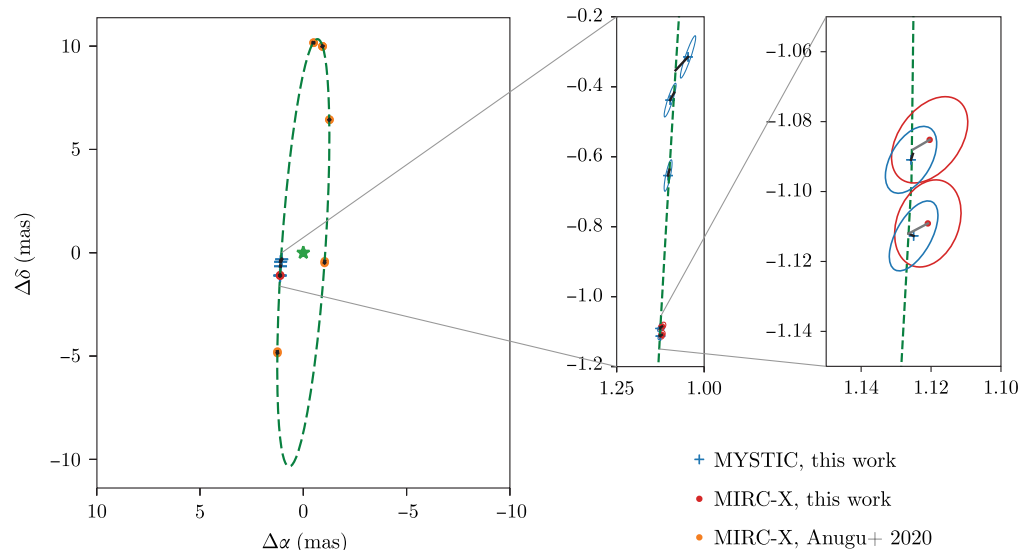


**Fig. 16** Binary separations with orbital parameters derived in Ref. 8 superimposed.

which we hope to correct with future improvements. We are in the process of optimizing the data reduction pipeline to provide data products with the required  $<2\%$  for square visibility and  $<0.1$  deg closure phase errors.

The optical train of MYSTIC implements a few refinements over the MIRC-X system, including an improved fiber injection system and a motorized filter wheel for fully automated operation. We hope to integrate these features into the MIRC-X beam train in the future. Progress is underway for co-phased observations with the forthcoming SPICA instrument,<sup>22</sup> which will extend simultaneous CHARA observations to visible wavelengths, and further improvements to MYSTIC's sensitivity are forthcoming.

A few avenues are still available to improve the sensitivity of the instrument in the near future, which we mention briefly here.

We have developed a pupil tracker, the Six Telescope Star Tracker (STST), to continuously monitor the CHARA beam drift, which was installed at CHARA in mid-August, 2022. We have inserted a beamsplitter into each of the CHARA IR beams, extracting 4% of the near infrared light. This light then directed into an 8 in. Newtonian telescope (Orion SkyQuest XT8) with its eyepiece removed. The beams are then tracked with a C-RED 2 camera from First Light, operating at 600 Hz, and the beam drift is corrected for by the CHARA lab-AO tip/tilt system. A pupil viewing lens is also made available via a small filter wheel prior to the camera. We are currently working to optimize the beam tracking software, though we optimistically anticipate a factor-of-two improvement in total photon coupling into the MYSTIC fibers once this system is operational.

Pending additional sources of funding for the instrument, we could replace the C-RED One camera for a newer version with a lower overall background.<sup>23</sup> MIRC-X and MYSTIC feature the first two commercially produced SAPHIRA detector-based cameras, and newer units resolve some early electronic tuning and isolation issues present in our cameras. For instance, new units are electronically isolated from the camera's cryo-pump and no longer exhibit a 94 Hz nuisance oscillation in the detector readout. Optimistically, a newer detector could provide an additional threefold improvement in sensitivity over the aforementioned upgrades.

Finally, we suspect that over half of the background flux measured on the detector originates from the warm sapphire window separating the MYSTIC cryostat from the camera's internal dewar. We plan to test this hypothesis by removing the window in the future, in preparation for a C-RED One camera upgrade. We note that this option does pose some additional risk to the camera, as any rapid pressure increase in the MYSTIC dewar may cause the camera filters to shatter and damage the detector.

These upgrades together could yield an upward of 2.7 magnitude sensitivity boost in the K-band, allowing regular observations of objects as faint as 10th magnitude. Such an improvement would enable imaging of hundreds of YSO (especially T Tauri) and a wide range of other targets, including high-mass x-ray binaries, novæ, and the brightest asymptotic giant branch (AGB) stars.

---

## Disclosures

The authors have no conflicts of interest to disclose, financial or otherwise.

## Data, Materials, and Code Availability

The data reduction pipeline is available at [https://gitlab.chara.gsu.edu/lebouquj/mircx\\_pipeline/](https://gitlab.chara.gsu.edu/lebouquj/mircx_pipeline/).

## Acknowledgments

MYSTIC is funded by the USA National Science Foundation Advanced Technologies and Instrumentation Program (PI: Monnier, Grant No. NSF-ATI 1506540). MIRC-X received funding from the European Research Council (ERC) under the European Union's Horizon 2020 Research and Innovation Program (Grant No. 639889). Additional funding for MIRC-X and MYSTIC was received through the following grants: NASA-XRP (Grant No. NNX16AD43G), NSF-AST (Grant No. 1909165), and NASA-MSGC (Grant No. NNX15AJ20H). B.R.S. and J.D.M. would like to acknowledge support by FINESST (NASA Grant No. 80NSSC19K1530). S.K. would also like to acknowledge support from an ERC Starting Grant (Grant No. 639889), ERC Consolidator Grant (Grant No. 101003096), and STFC Consolidated Grant (Grant No. ST/V000721/1). We thank external members of the MYSTIC design review committee for their recommendations, namely: Antoine Mérand, Jean-Philippe Berger, Michael Ireland, Denis Mourard, and Judit Sturmman. We would like to thank GRAVITY collaboration for their support and approval to use the spare ABCD integrated optics combiners within MYSTIC. We additionally thank IPAG for material and lab support to prepare the chip for this instrument. This work includes observations obtained with the Georgia State University Center for High Angular Resolution Astronomy Array at Mount Wilson Observatory. The CHARA Array is supported by the National Science Foundation (Grant Nos. AST-1636624 and AST-2034336). Institutional support has been provided from the GSU College of Arts and Sciences and the GSU Office of the Vice President for Research and Economic Development. Much of this manuscript originally appeared in SPIE Proceedings Volume 12183, Optical and Infrared Interferometry and Imaging VIII; 121830B (2022) <https://doi.org/10.1117/12.2629437>.

## References

1. T. A. ten Brummelaar et al., “First results from the CHARA Array. II. A description of the instrument,” *Astrophys. J.* **628**, 453–465 (2005).
2. X. Che et al., “Optical and mechanical design of the CHARA Array adaptive optics,” *J. Astron. Instrum.* **2**, 1340007 (2013).
3. T. A. ten Brummelaar et al., “The CHARA Array adaptive optics program,” *Proc. SPIE* **10703**, 1070304 (2018).
4. N. Anugu et al., “CHARA Array adaptive optics: complex operational software and performance,” *Proc. SPIE* **11446**, 1144622 (2020).
5. J. D. Monnier et al., “Michigan Infrared Combiner (MIRC): commissioning results at the CHARA Array,” *Proc. SPIE* **6268**, 62681P (2006).
6. G. Finger et al., “SAPHIRA detector for infrared wavefront sensing,” *Proc. SPIE* **9148**, 914817 (2014).
7. C. Lanthermann et al., “Modeling the e-APD SAPHIRA/C-RED ONE camera at low flux level. An attempt to count photons in the near-infrared with the MIRC-X interferometric combiner,” *Astron. Astrophys.* **625**, A38 (2019).
8. N. Anugu et al., “MIRC-X: a highly sensitive six-telescope interferometric imager at the CHARA Array,” *Astron. J.* **160**, 158 (2020).
9. S. J. Kenyon and L. Hartmann, “Pre-main-sequence evolution in the taurus-auriga molecular cloud,” *Astrophys. J. Suppl.* **101**, 117 (1995).
10. T. Gardner et al., “ARMADA. I. Triple companions detected in B-type binaries  $\alpha$  Del and  $\nu$  Gem,” *Astron. J.* **161**, 40 (2021).
11. K. Perraut et al., “Single-mode waveguides for GRAVITY. I. The cryogenic 4-telescope integrated optics beam combiner,” *Astron. Astrophys.* **614**, A70 (2018).

12. N. J. Scott et al., “Jouvence of fluor: upgrades of a fiber beam combiner at the CHARA Array,” *J. Astron. Instrum.* **2**, 1340005 (2013).
13. Gravity Collaboration et al., “First light for GRAVITY: phase referencing optical interferometry for the Very Large Telescope Interferometer,” *Astron. Astrophys.* **602**, A94 (2017).
14. B. R. Setterholm et al., “MIRC-X polarinterferometry at CHARA,” *Proc. SPIE* **11446**, 114460R (2020).
15. T. A. Ten Brummelaar et al., “The classic/climb beam combiner at the CHARA Array,” *J. Astron. Instrum.* **2**, 1340004 (2013).
16. B. Lazareff, J. B. Le Bouquin, and J. P. Berger, “A novel technique to control differential birefringence in optical interferometers. Demonstration on the PIONIER-VLTI instrument,” *Astron. Astrophys.* **543**, A31 (2012).
17. L. Sturmman et al., “Nine-channel tip/tilt detector at the CHARA Array,” *Proc. SPIE* **6268**, 62683T (2006).
18. S. B. Shaklan and F. Roddier, “Single-mode fiber optics in a long-baseline interferometer,” *Appl. Opt.* **26**, 2159–2163 (1987).
19. J. L. Gach et al., “C-RED one: ultra-high speed wavefront sensing in the infrared made possible,” *Proc. SPIE* **9909**, 990913 (2016).
20. A. Chelli et al., “Pseudomagnitudes and differential surface brightness: application to the apparent diameter of stars,” *Astron. Astrophys.* **589**, A112 (2016).
21. M. Konacki et al., “High-precision orbital and physical parameters of double-lined spectroscopic binary stars—HD78418, HD123999, HD160922, HD200077, and HD210027,” *Astrophys. J.* **719**, 1293–1314 (2010).
22. D. Mourard et al., “CHARA/SPICA: a six-telescope visible instrument for the CHARA Array,” *Proc. SPIE* **12183**, 1218308 (2022).
23. P. Feautrier and J.-L. Gach, “Last performances improvement of the C-RED One camera using the 320x256 e-APD infrared Saphira detector,” *Proc. SPIE* **12183**, 121832E (2022).

**Benjamin R. Setterholm** received his BS degree in astrophysics and BE degree in aerospace engineering from the University of Minnesota in 2016 and his MS and PhD degrees in astronomy and astrophysics from the University of Michigan in 2018 and 2022, respectively. He is an assistant research scientist at the University of Michigan. He is currently involved in the development of data processing and analysis routines for the forthcoming NASA SunRISE mission.

**John D. Monnier** received his BS degree in physics from Purdue in 1993 and his PhD in physics from the UC Berkeley in 1999. Since 2002, he has been a professor at the University of Michigan. He is interested in all stages of stellar and planetary evolution, with a focus on imaging surfaces of stars and planet-forming disks along with development of methods for extrasolar planet detection. He was the PI of the Michigan InfraRed Combiner and Michigan Young STar Imager at CHARA (MYSTIC). He received the 2019 AAS Joseph Weber Award for Astronomical Instrumentation.

**Jean-Baptiste Le Bouquin** received his PhD in astrophysics in 2005 from the Université Joseph Fourier in Grenoble, France, where he currently works as an associate astronomer. He was first to demonstrate a K-band integrated optics device in astronomical interferometry and was the PI for the four-telescope VLTI combiner PIONIER and the VLTI-AT NAOMI AO systems. He also played critical roles in developing the GRAVITY instrument at VLTI and MIRC-X and MYSTIC at CHARA.

**Narsireddy Anugu** received his PhD in astronomical instrumentation from the Faculty of Engineering, University of Porto, Portugal, in 2017. He is a staff scientist at the CHARA Array, Georgia State University, United States. His current research interests include astronomical interferometry, adaptive optics, and binary stars.

**Jacob Ennis** received his BS degree in physics from the University of Michigan in 2019. He was heavily involved in the design, fabrication, and commissioning of key subsystems within MIRC-X and MYSTIC as well as the CHARA STS and STST assemblies. He is currently pursuing his MS degree in computer science at Arizona State University.

**Laurent Jocou** received his MSc degree in instrumentation and optics. He was involved at Observatoire de Paris in the development of fiber links dedicated to the FLAME/ESO spectrograph. In 2001, he joined the Institut de planetologie et d’Astropysique de Grenoble (IPAG) to develop interferometric combiners and later contributed to the development of the GRAVITY beam combiners. Currently, he is involved in the development of a subsystem to perform high-contrast imaging on the HARMONI/ELT instrument.

**Nour Ibrahim** received her BS degree in astronomy from Embry-Riddle Aeronautical University in 2020 and her MS degree in astronomy and astrophysics from the University of Michigan in 2022. She is a PhD student at the University of Michigan. She uses long baseline interferometry, mainly using the CHARA Array, to image and model the inner 1-au regions of planet-forming disks around young stars.

**Stefan Kraus** is a professor of astrophysics at the University of Exeter. His group conducts studies on fundamental stellar astrophysics and exoplanets and planet formation and drives the development of infrared interferometry instrumentation. Before moving to Exeter in 2013, he held a NASA Sagan fellowship at Michigan and fellowships at the Harvard-Smithsonian Center for Astrophysics and at the Max-Planck-Institute at Bonn, where he also received his PhD. His work has been recognized with an Otto Hahn Medal by the Max Planck Society and a Philip Leverhulme prize and received support through two European Research Council grants.

**Matthew D. Anderson** received his PhD in astronomy from Georgia State University in 2022. He is a postdoctoral research associate at the CHARA Array responsible for the beam combination laboratory and the adaptive optics program. His research interests include active galactic nuclei and control algorithms for adaptive optics.

**Sorabh Chhabra** received his PhD in speckle interferometry techniques and instrument development from IUCAA, Pune, India, in 2022. He is a postdoctoral research associate at the University of Exeter, UK. He is responsible for the design of spectrograph for the upcoming VLTI visiting instrument BIFROST. He is broadly interested in astronomical instrumentation with applications in adaptive optics, speckle interferometry, and long baseline interferometry.

**Isabelle Codron** received her MPhys degree in physics with astrophysics from the University of Exeter in 2021. She is a PhD student at the University of Exeter. Her research is on using long-baseline interferometry to image the inner region of protoplanetary discs with her current focus on disc warping and misalignments.

**Christopher D. Farrington** received his PhD in astronomy from Georgia State University in 2008. He is the chief operations scientist at the CHARA Array where he has been since 2006. From 2006 to 2018, he served as the lead operator of the array and took on the role of head of operations in 2018. His research interests include double stars, fundamental stellar parameters, and engineering design for the mobile seventh telescope for the CHARA Array.

**Becky Flores** is a graduate student in the Physics and Astronomy Department at Georgia State University. Her research uses the CHARA Array to measure angular diameters of stars that have dynamical masses to study evolution of solar-like to low mass main sequence stars.

**Tyler Gardner** is a postdoctoral researcher at the University of Exeter, having recently received his PhD in astronomy and astrophysics from the University of Michigan. His research focuses on using long-baseline interferometry for precision astrometry, exoplanet detection and characterization, and studying binary/multiple star systems. He is the PI of multiple observing programs at VLTI and CHARA Arrays.

**Mayra Gutierrez** is an undergraduate student at the University of Michigan studying astronomy and physics. She assisted in designing and fabricating the CHARA STST assembly. Her current research is in formation flying space interferometry and she will graduate with her BS degree in 2024.

**Cyprien Lanthermann** obtained his PhD from the Université Grenoble Alpes working on the implementation of the e-APD detector of MIRC-X and MYSTIC, and using these instruments to study the multiplicity of massive stars. He worked for 1 year at KU Leuven on the study of massive stars and the early study of the MARVEL spectroscopic facility and is now working at the CHARA Array on the implementation of the Silmaril instrument and is the visitor support scientist there.

**Olli W. Majoinen** has been an research technician and array telescope operator at CHARA since 2015. He has been involved in observational astronomy since the '90s, operating local observatories in Finland and Australia.

**Daniel J. Mortimer** received his master's degree from the University of Leeds and his PhD from the University of Cambridge. He is a postdoctoral research fellow at the University of Exeter, where he specialises in the design of near-infrared beam combiners for long baseline optical interferometers.

**Gail Schaefer** is the director of the CHARA Array of Georgia State University. She leads the CHARA staff and oversees the community access program at the Array. Her research focuses on mapping the orbits of binary stars using long-baseline interferometry and adaptive optics imaging. She received her PhD in physics and astronomy from Stony Brook University in 2004.

**Nicholas J. Scott** received his PhD in astronomy from Georgia State University and the Observatoire de Paris, in 2015. He is the telescope systems scientist at the CHARA Array. His main research interests are exozodiacal dust and its evolution, high angular resolution optical and near-IR instrumentation, speckle and long baseline optical interferometry, exoplanets, stellar astrophysics, hardware development, prototyping, and instrumentation. In addition to instrumentation, he has extensive teaching experience and has a strong interest in public outreach.

**Theo ten Brummelaar** received his PhD from the University of Sydney in 1993, where he worked on the Sydney University Stellar Interferometer under the supervision of Dr. William Tango. He then moved to Atlanta, Georgia, as a postdoctoral research associate working under Dr. Harold MacAlister on the early development of the CHARA Array at Georgia State University. He remained at the CHARA Array, eventually becoming the director of the CHARA Array until his retirement in 2022.

**Norman L. Vargas** has been a research technician at the CHARA Array since 2012 where his primary duty is operating the array telescopes as a night assistant. His previous astronomical and telescope experience includes operating the 60 and 100 in. telescopes for the Mount Wilson Observatory since 2000 and public outreach with the Los Angeles Astronomical Society.